AGU PUBLICATIONS

Geophysical Research Letters

RESEARCH LETTER
10.1002/2016GL067805

Key Points:
- First identification of strike-slip faulting on Enceladus outside of the south polar terrain
- Strike-slip faults on Enceladus are uncharacteristic for strike-slip faults on other icy bodies
- Strike-slip faulting on Enceladus is controlled by a fundamentally different process than on Europa

Supporting Information:
- Supporting Information S1

Correspondence to:
E. S. Martin,
martines@si.edu

Citation:
Martin, E. S. (2016), The distribution and characterization of strike-slip faults on Enceladus, *Geophys. Res. Lett.*, *43*, 2456–2464, doi:10.1002/2016GL067805.

Received 15 JAN 2016
Accepted 8 MAR 2016
Accepted article online 11 MAR 2016
Published online 24 MAR 2016

The distribution and characterization of strike-slip faults on Enceladus

Emily S. Martin[1,2]

[1]Center for Earth and Planetary Studies, National Air and Space Museum, Smithsonian Institution, Washington, District of Columbia, USA, [2]Department of Geological Sciences, University of Idaho, Moscow, Idaho, USA

Abstract Strike-slip faulting is typically characterized by lateral offsets on icy satellites of the outer solar system. However, strike-slip faults on Enceladus lack these typical lateral offsets and instead are marked by the presence of tailcracks or en echelon cracks. These features are used here to develop the first near-global distribution of strike-slip faults on Enceladus. Strike-slip faults on Enceladus fall into three broad categories: tectonic terrain boundaries, reactivated linear features, and primary strike-slip faults. All three types of strike-slip faults are found predominantly, or within close proximity to, the antipodal cratered terrains on the Saturnian and anti-Saturnian hemispheres. Stress modeling suggests that strike-slip faulting on Enceladus is not controlled by nonsynchronous rotation, as on Europa, suggesting a fundamentally different process driving Enceladus's strike-slip faulting. The motion along strike-slip faults at tectonic terrain boundaries suggests large-scale northward migration of the ice shell on the leading hemisphere of Enceladus, occurring perpendicular to the opening direction of the tiger stripes in the south polar terrain.

1. Introduction

Lateral motion is an important component in the deformation of icy shells and has played a role in modifying the surfaces of icy bodies including Europa [*Hoppa et al*., 1999; *Kattenhorn*, 2004; *Sarid et al*., 2002], Ganymede [*Pappalardo et al*., 1998], Enceladus [*Smith-Konter and Pappalardo*, 2008; *Hurford et al*., 2007, 2012], and possibly Triton [*Smith et al*., 1989; *Croft et al*., 1995] (Figure 1). Strike-slip faulting has been observed almost exclusively within Enceladus's south polar terrain (SPT) composed of four prominent "tiger stripes" [*Porco et al*., 2006] that source jet activity [*Spitale and Porco*, 2007], and "paleo" tiger stripes [*Patthoff and Kattenhorn*, 2011] encircled by the southern curvilinear terrains [e.g., *Crow-Willard and Pappalardo*, 2015]. The tiger stripes likely formed due to a global stress field induced by nonsynchronous rotation (NSR) [*Patthoff and Kattenhorn*, 2011]. Strike-slip motions along the tiger stripes are generated by tidal stresses [*Nimmo et al*., 2007; *Hurford et al*., 2007] caused by changes in Enceladus's tidal bulge due to its eccentric orbit. Until now, only cursory analyses of strike-slip faults have been attempted outside of the SPT [*Kargel and Pozio*, 1996].

Fracture patterns preserved in icy shells can be used to identify the stress mechanism(s) from which they formed and may include polar wander, despinning, shell volume changes, orbital recession/decay, diurnal tidal factors, NSR [*Kattenhorn and Hurford*, 2009; *Collins et al*., 2010], obliquity, libration, and precession [*Rhoden et al*., 2012]. The global pattern of strike-slip faults on Europa has been attributed to diurnal tidal stresses and NSR [*Hoppa et al*., 1999; *Sarid et al*., 2002; *Kattenhorn*, 2004; *Rhoden et al*., 2011]. The distribution of strike-slip faults on Europa revealed a prevalence of right-lateral strike-slip faults in the southern hemisphere and predominantly left-lateral strike-slip faults in the northern hemisphere [*Hoppa et al*., 1999]. Recent work suggests that stress models produce an improved fit to the observed strike-slip fault distribution on Europa when polar wander, obliquity, libration, or precession are also considered [*Rhoden et al*., 2011, 2012; *Rhoden and Hurford*, 2013]. Processes shown to affect strike-slip faults on Europa, like diurnal tidal forcing and NSR, may also drive strike-slip fault formation on Enceladus outside of the SPT.

Strike-slip faults on Enceladus outside of the SPT lack the characteristic lateral offsets observed on other icy moons (Figure 1), and their distribution, morphology, and formation have not been previously explored. Diagnostic secondary structures (e.g., tailcracks (section 2.1) and en echelon cracks (section 2.2)) (Figure 2) are typical of strike-slip faults and can be used to identify strike-slip faults and their slip sense [*Kattenhorn*, 2004; *Groenleer and Kattenhorn*, 2008; *Pollard et al*., 1982] in the absence of offsets and are used to identify, characterize, and constrain the stress conditions at the time of formation.

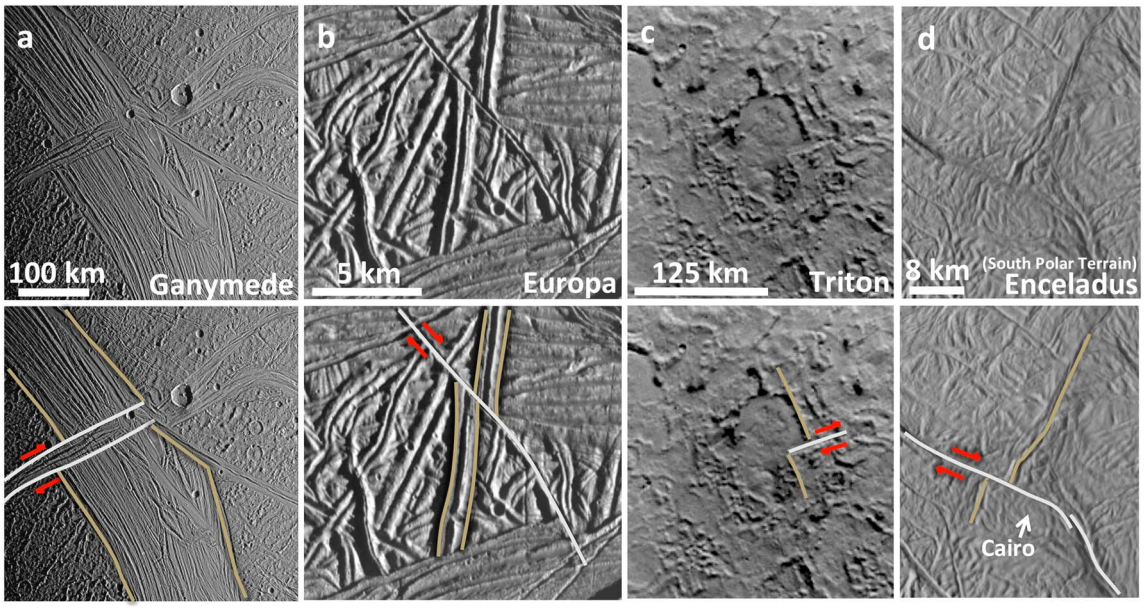

Figure 1. Examples of strike-slip faults with lateral offsets on (a) Ganymede (Image PIA01619) and (b) Europa (Image PIA00849), (c) possible strike-slip fault on Triton (PIA02216) [e.g., *Smith et al*., 1989, Figure 32; *Croft et al*., 1995], and (d) Enceladus's south polar terrain. SPT mosaic by *Roatsch et al*. [2013]. Lateral offsets are characteristic of strike-slip faults on icy bodies of the outer solar system except outside of Enceladus's SPT.

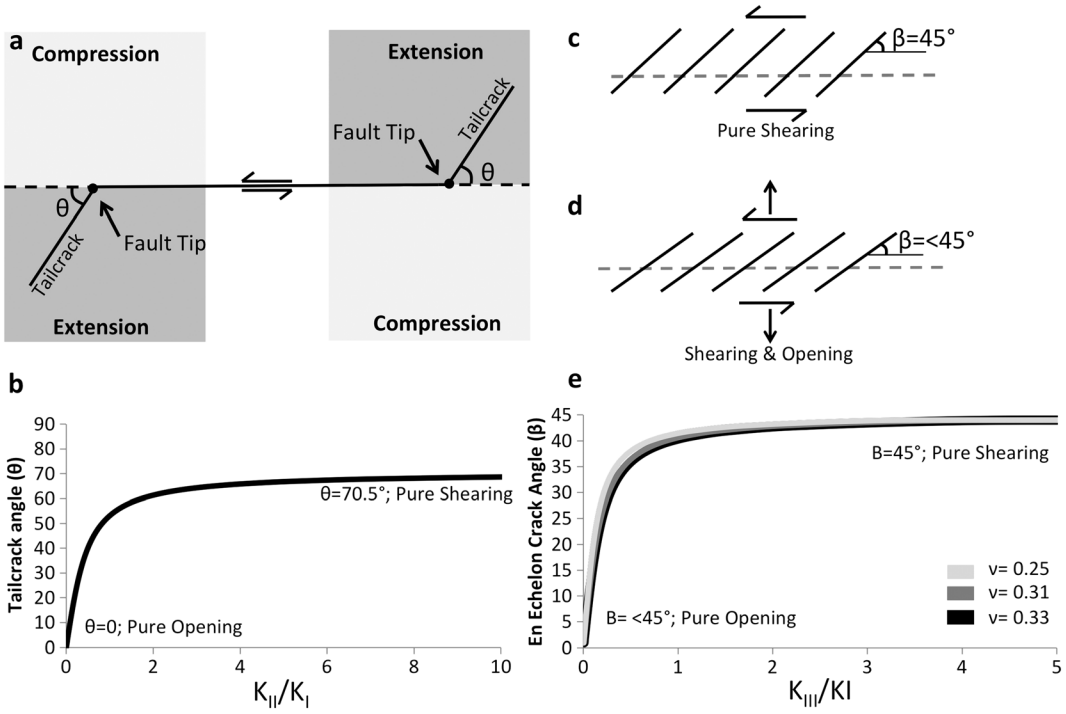

Figure 2. (a) Tailcracks are tension cracks that can form at fault tips. θ is the tailcrack angle [after *Kattenhorn*, 2004]. (b) Predicted tailcrack angles as a function of the ratio of stress intensity factors of opening (K_I) and shearing (K_{II}). (c) En echelon cracks over a strike-slip fault form at $\beta = 45°$ to strike. (d) $\beta < 45°$ if a component of opening exists [*Olson and Pollard*, 1991; *Cruikshank et al*., 1991]. (e) The ratio of shear to opening can be predicted from β assuming a ν (Poisson's ratio). See also Text S3.

2. Strike-Slip Faulting

Broadly, strike-slip faults will occur when the intermediate tensile stress (σ_2) is vertical with either right- or left-lateral displacement [*Anderson*, 1951]. No net extension or contraction of the crust occurs unless there is an oblique component of motion along the fault. On Earth, strike-slip faults can form transform plate boundaries, or act as linking features between extending terrains such as mid-ocean ridges and continental rift zones.

Strike-slip faults manifested as offsets are ubiquitous on Europa [e.g., *Kattenhorn*, 2002, 2004] and Ganymede (Figure 1) but are not generally observed outside of the SPT on the surface of Enceladus. The paucity of offsets suggests a fundamentally different process driving strike-slip faulting on Enceladus.

2.1. Tailcracks

Tailcracks (also referred to as wing cracks, kinks, and horsetail fractures) [*Cruikshank et al*., 1991; *Willemse et al*., 1997] are secondary tension cracks [*Pollard and Aydin*, 1988; *Cruikshank et al*., 1991] which form at the tips of strike-slip faults and can be used to identify the sense of slip of a fault [*Kattenhorn*, 2004; *Kattenhorn and Marshall*, 2006; *Groenleer and Kattenhorn*, 2008] (Figures 2a and 2b). The tailcrack angle (θ) is the angle between the intersection of the tailcrack and the fault plane. Theoretically, $\theta = 70.5°$ for a fault experiencing pure shear, and $\theta = 0°$ for a fault experiencing pure opening [*Erdogan and Sih*, 1963; *Lawn and Wilshaw*, 1975; *Pollard and Segall*, 1987]. Deviations from $\theta = 70.5°$ are used to infer the relative amounts of opening and shearing occurring along these faults (Figure 2b). *Kattenhorn* [2004] used tailcrack geometries on Europa to identify strike-slip motion and to infer that dilation was a significant concurrent component of motion along many strike-slip faults. Similarly, tailcracks on Enceladus are assumed to indicate shear motion along a fault.

2.2. En Echelon Cracks

En echelon cracks are often observed at the terminations of sheared joints [*Cruikshank and Aydin*, 1995] and can occur as a peripheral breakdown fringe along the edges of a parent crack (e.g., joints, veins, and igneous intrusions) in response to a rotation of the principal stresses during the growth process [*Pollard et al*., 1982; *Sommer*, 1969; *Nicholson and Pollard*, 1985]. An array of en echelon cracks is interpreted as the surface manifestation of a subsurface strike-slip fault (Figure 2c), as is commonly observed along terrestrial subsurface strike-slip faults. En echelon cracks forming above a subsurface shear fracture undergoing purely strike-slip motions will have an en echelon angle (β) of 45°, the angle between the strike of the subsurface fault and the echelon crack [*Ramsay*, 1980; *Olson and Pollard*, 1991] (Figures 2c–2e). If a component of fault-perpendicular tension and dilation is present, then $\beta < 45°$ (Figure 2d). Arrays of en echelon cracks are known to be a type of Riedel fracture called a T fracture, forming as the result of subsurface shear [*Riedel*, 1929; *Cloos*, 1955] (Text S1 and Figure S1). T fractures are distinct from other en echelon fractures that can develop in shear zones, because of the characteristic angle at which Riedel shears form (Figure S1).

3. Strike-Slip Fault Distribution and Classification

Twenty-one individual strike-slip faults were identified across Enceladus (Figures 3 and S2 and Text S2). No preferential fault orientation or length was observed. Strike-slip faults are located primarily within the cratered terrains between 120°E and 120°W and between 60°W and 60°E. There is an absence of strike-slip faults within the tectonized terrains near 90°W and 90°E and within the polar regions north and south of 60°N and 60°S. The paucity of strike-slip faults in the north polar region may be a result of limited data coverage (Figure S2 and Text S2). There is no preference for left-lateral or right-lateral strike-slip faults in either the northern or southern hemispheres, nor are there morphologic equivalents for Europa's band-like strike-slip faults [*Kattenhorn*, 2004] (e.g., Figure 1b).

Among the 21 mapped strike-slip faults, 3 classes of faults were identified and characterized: (1) those defining major tectonic terrain boundaries (Figures 4a and 4b), (2) reactivated linear features (Figure 4c), and (3) primary strike-slip faults (Figures 4d and 4e). Tectonic terrain boundaries comprise 24% of the strike-slip faults, 38% are reactivated linear features, and 38% are primary strike-slip faults (Figure 3b). Hereafter, faults are identified by unique numbers from Figure 3 as [*n*].

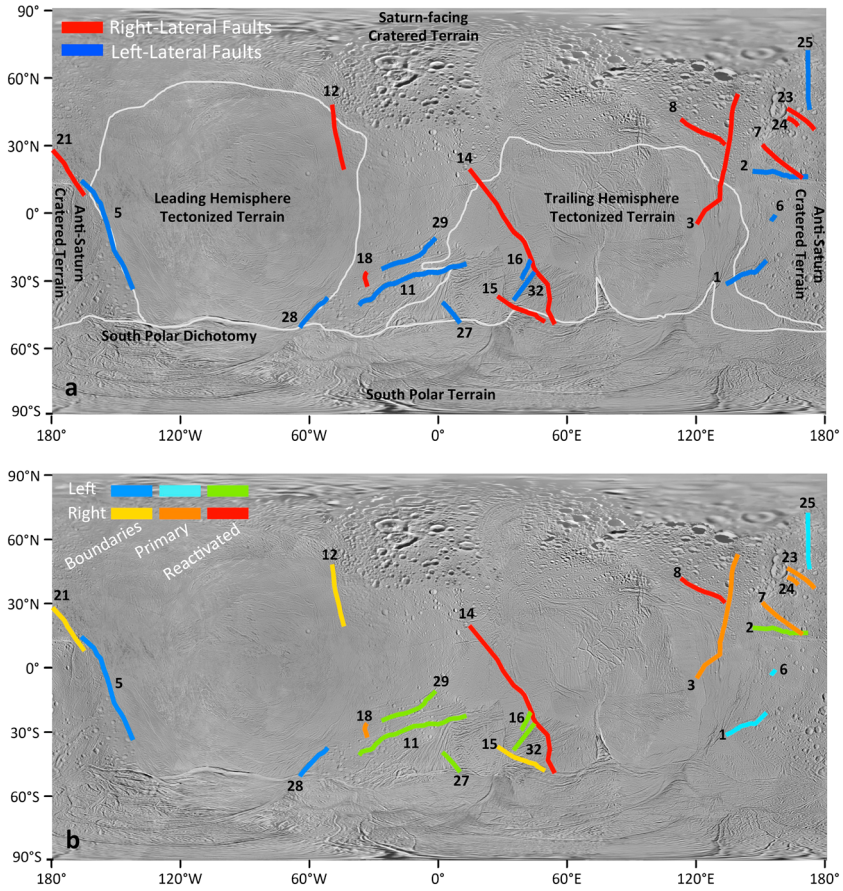

Figure 3. The global distribution of strike-slip faults on Enceladus. (a) Red and blue indicate right- and left-lateral strike-slip faults, respectively. Unique numbers identify each fault (Table S1). (b) Strike-slip fault classification for left- and right-lateral strike-slip faults (cool and warm tones, respectively): tectonic terrain boundaries (dark blue; yellow), primary strike-slip faults (light blue; orange), and reactivated linear features (green; red). Global mosaic by *Roatsch et al.* [2013] (see also Text S2 and Figure S2).

3.1. Tectonic Terrain Boundary Strike-Slip Faults

Close examination of abrupt boundaries between Enceladus's tectonized and cratered terrains reveals zones of en echelon fractures. Tectonic terrain boundaries (Figures 4a and 4b) delineate the leading hemisphere tectonized terrain from the Saturn and anti-Saturn cratered terrains with both left-lateral [5] and right-lateral [12, 21] faults. Two tectonic terrain boundary faults intersect the southern curvilinear terrains: a left-lateral fault at 60°W [28] and a right-lateral fault at 60°E [15] extend from the southern curvilinear terrains into the trailing hemisphere tectonized terrains.

3.2. Reactivated Linear Features

A reactivated linear feature is a fracture that experienced shear motion after its initial formation (Figure 4c). Evidence for the reactivation of preexisting faults suggests multiple stages of motion indicative of a changing stress field. The reactivated linear feature in Figure 4c shows two tectonic episodes: (1) the zone of broad troughs or furrows accommodating extension and (2) shear motion forming tailcracks on the eastern end of these furrows. The zone of extension preceded the formation of tailcracks due to a change in the stress field. If they formed concurrently, the amount of opening along the furrows would have resulted in tailcracks with much lower angles (Figure 2b). Evidence for the reactivation of preexisting faults indicates multiple stages of motion indicative of a changing stress field.

A higher concentration of left-lateral reactivated linear features occurs in the southern hemisphere of Saturn-facing cratered terrains (Figure 3b). Faults [29] and [11] (both left-lateral) are associated with swaths of continuous tectonized terrains crossing into the Saturn-facing cratered terrains. To the east of this group

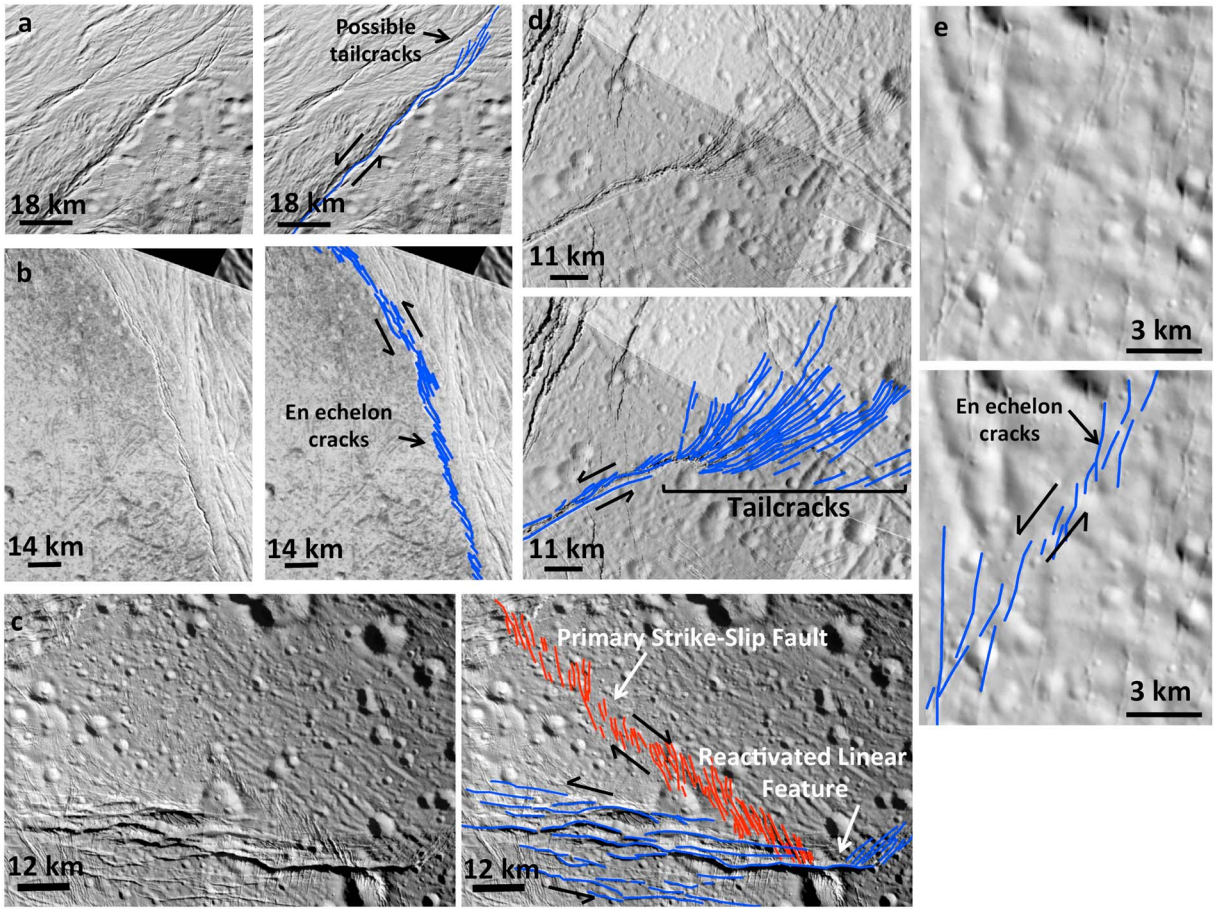

Figure 4. Classification of strike-slip faults on Enceladus. (a) Tectonic terrain boundary separating cratered terrain from tectonic terrain, centered at 58°W and 44°S (Fault [28] in Figure 3). Image No. N1660434444. (b) Tectonic terrain boundary centered at 153°W and 6°S (Fault [5]), identified as a series of en echelon cracks. Image No. N167591706. (c) Crosscutting strike-slip faults centered at 158°E and 17°N. (Faults [2, 7]) Image No. N1489050254. (d) Primary strike-slip fault at 145°E, 26°S, with characteristic tailcracks. (Fault [1]) Image No. N1500061771. (e) Primary strike-slip fault as an array of right-stepping, en echelon cracks at 156°E, 2°S. (Fault [6]) Image No. N1489050475.

of left-lateral faults is a right-lateral, reactivated fault [14]. This is the longest strike-slip fault mapped (350 km long and is composed of four 50–100 km segments). Only two reactivated features occur within close proximity to the anti-Saturn cratered terrains [2, 8].

3.3. Primary Strike-Slip Faults

Primary strike-slip faults are those that initially broke through the surface as the manifestation of a subsurface shear fracture. Primary strike-slip faults are distinguished from "reactivated linear features" in that the breakthrough to the surface occurred during shearing, as opposed to shearing of a feature already present at the surface. They have not experienced any subsequent reversal of slip direction. Primary strike-slip faults developing in response to the reactivation of ancient subsurface or heavily mantled faults cannot be ruled out. However, if reactivation of an inherited crustal fabric (preexisting structures) is involved in the development of primary strike-slip faults, it would be indistinguishable.

The highest concentration of primary strike-slip faults are near the anti-Saturn cratered terrains (Figure 3b), with seven primary strike-slip faults, in contrast to the one primary strike-slip fault on the Saturn-facing cratered terrains. Additionally, the primary strike-slip faults in the anti-Saturn cratered terrains are generally north of the equator. This is in contrast to reactivated linear features, which are predominantly found south of the equator in the Saturn-facing cratered terrains. Fault [25] is a primary left-lateral strike-slip fault that can be traced into the north polar region (Figure S3).

4. Strike-Slip Faults in an NSR Stress Field

The presence of tailcracks and en echelon cracks associated with strike-slip faults can be used to infer relative amounts of shear and opening that occurred along the fault when secondary fractures formed [*Kattenhorn*, 2004; *Pollard et al*., 1982]. The ratio of shear to opening (Texts S3 and S4), derived from observations (Table S1), can be compared with similar ratios generated from models (e.g., Figure S4) to identify the stress mechanisms that formed the strike-slip fault. Either tailcrack angles or en echelon crack angles (Figure 2) were measured along mapped strike-slip faults on Enceladus in a Mercator projection, reprojected about the center of each fault.

Geologic evidence suggests diurnal tidal stresses, and NSRs are likely occurring on Enceladus [*Patthoff and Kattenhorn*, 2011; *Hurford et al*., 2007, 2012]. However, diurnal stresses in the SPT are unlikely to exceed ~80 kPa [*Smith-Konter and Pappalardo*, 2008] and insufficient to overcome the tensile strength of ice (~1–3 MPa [*Schulson and Duvall*, 2009]). Additionally, fractures that form as the result of diurnal stresses may be arcuate, like the cycloids found on Europa [*Marshall and Kattenhorn*, 2005; *Groenleer and Kattenhorn*, 2008], but thus far have not observed on Enceladus. Outside the SPT the ice shell is likely thicker and diurnal stresses would be lower than those observed in the SPT [e.g., *Smith-Konter and Pappalardo*, 2008] and are less likely to initiate fracturing within the ice shell. Nonetheless, diurnal stresses may be sufficient to drive motion along preexisting fractures, as has been suggested for controlling the timing of jet activity in the SPT [*Hurford et al*., 2007, 2012*; Porco et al*., 2014; *Nimmo et al*., 2014].

The magnitude of diurnal stresses are likely insufficient to fracture Enceladus's ice shell. Stresses induced only by NSR were compared with observational constraints on strike-slip faults on Enceladus. For each measurement of θ or β, the ratio of the stress intensity factors $K_{II(III)}/K_I$ was calculated (Text S3). Using SatStressGUI [*Kay*, 2010; *Wahr et al*., 2009; *Patthoff et al*., 2015] the ratio of shear to normal stresses (σ_s/σ_n) (Text S4) was calculated over 180° of longitude within the modeled NSR stress field (Figures S4b and S4d). For longitudes where $\sigma_s/\sigma_n \approx K_{II(III)}/K_I$, the observed slip sense of the fault must match the orientation of the NSR stresses local to the fault (Table S1). If the sense of slip induced by modeled NSR stresses matches the observed slip sense, then it is possible that the particular strike-slip fault formed in an NSR stress field at that longitude, like faults [1, 2]. For fault [1], $\sigma_s/\sigma_n = -0.6$ and $K_{II}/K_I = -0.82$ at 81.18°W (Table S1) in an NSR stress field (Figure S5) and would produce left-lateral motion, consistent with the observed slip sense. For fault [2], $\sigma_s/\sigma_n = -0.39$ and $K_{II}/K_I = -0.69$ at 65.65°W (Table S1), producing slip consistent with the observed left-lateral motion. Fourteen strike-slip faults were found where $\sigma_s/\sigma_n \approx K_{II(III)}/K_I$, but only two [1, 2] strike-slip faults had a slip sense consistent with having formed in an NSR stress field.

5. Discussion

The distribution of strike-slip faults on Enceladus reveals a dearth of strike-slip faults within the tectonized terrains. The broadly antipodal nature of the global strike-slip fault distribution is similar to that of the global distribution of features called pit chains [*Michaud et al*., 2008]. Pit chains form by the drainage of loose material into a dilational crack or subsurface normal fault [*Michaud et al*., 2008; *Wyrick et al*., 2004]. Pit chains, unlike strike-slip faults, are likely forming in response to NSR stresses [*Martin and Kattenhorn*, 2014], suggesting that there are multiple stress mechanisms driving tectonic activity on Enceladus. The near-global distribution of strike-slip faults and global distribution of pit chains is not the result of observational biases; the distribution may indicate differences in ice shell thickness or inherited crustal weaknesses (remnants of previous geologic activity), between cratered and tectonized terrains within the ice shell.

NSR should produce predominantly left-lateral strike-slip faults in the northern hemisphere and right-lateral strike-slip faults in the southern hemisphere [*Hoppa et al*., 1999]. Not only is this pattern not observed on Enceladus but also a NSR stress field cannot explain long strike-slip faults (e.g., [3], [5], and [14]) that cross the equator with a consistent sense of slip.

Motions along faults [5, 25, and 12] are suggestive of large-scale motion of the brittle portion of the ice shell and the opening of the tiger stripes (Figures 5 and S3). This does not imply that faults [5, 25, and 12] formed contemporaneously. Rather, recent motion along these faults occurred simultaneously. The funiscular or "ropy" terrains between the tiger stripes in the SPT are composed of short wavelength, subparallel features interpreted to be folds [*Spencer et al*., 2009; *Barr and Preuss*, 2010; *Bland et al*., 2015]. If the funiscular terrains

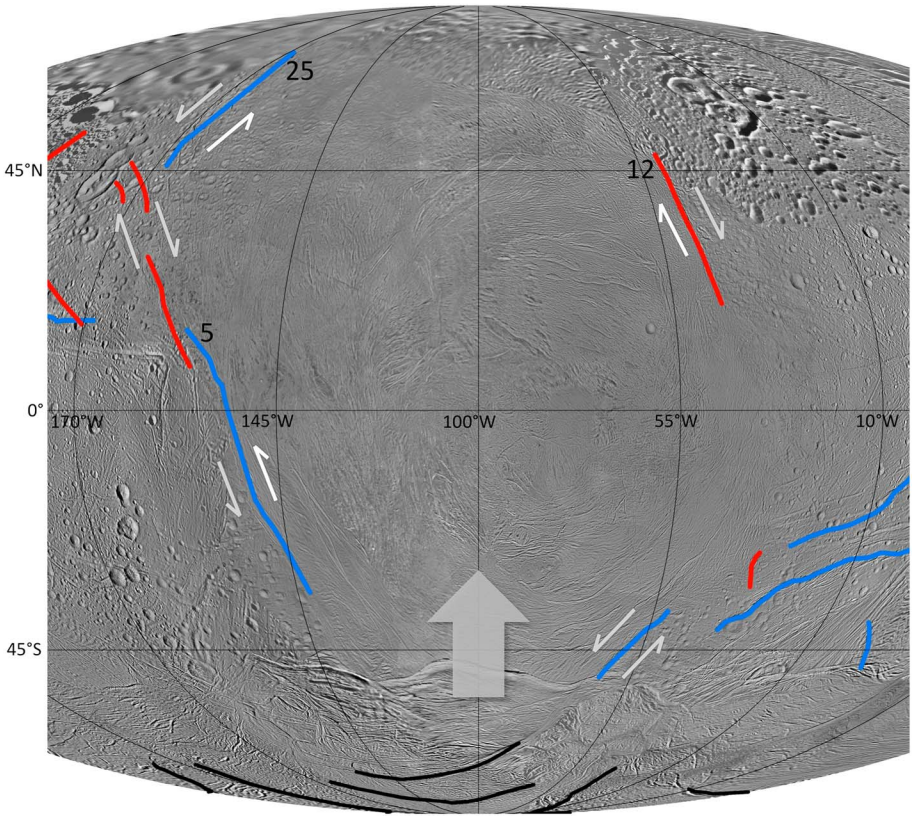

Figure 5. Left-lateral faults [5, 25] (Figure 3a) and right-lateral fault [12] drive a net northward motion of the leading hemisphere tectonized terrains, perpendicular to the opening direction of the tiger stripes. Tiger stripes (black) are highlighted in the south polar region. Mollweide projection.

are the result of compression due to opening along the tiger stripes, they may also be driving the leading hemisphere tectonized terrains northward, consistent with the observed opposing sense of slip along tectonic terrain boundary strike-slip faults [5, 25, and 12]. Faults [28, 21, 23, and 24] appear to be inconsistent with this interpretation; however, [28] is closely associated with the dynamic southern curvilinear terrains [e.g., *Crow-Willard and Pappalardo*, 2015; *Yin and Pappalardo*, 2015] and is likely locally influenced by the southern curvilinear terrains rather than large-scale crustal motions. Similarly, faults [21, 23, and 24] may be driven by the westward offset from faults [5 and 25]. Further work will be necessary to verify the motion of the leading hemisphere tectonized terrains.

The fracture patterns and geologic activity within the SPT on Enceladus were previously inferred to be the result of stresses induced by both NSR and diurnal tidal deformation [*Patthoff and Kattenhorn*, 2011]. If these same mechanisms are the main control on the global strike-slip fault pattern on Europa, then the lack of a match between strike-slip patterns on Europa and Enceladus is intriguing. Other mechanisms may be at work on Europa, as shown by *Kattenhorn* [2004], which noted that only band-like strike-slip faults (Figure 1b) follow the tidal walking model presented for Europa [*Hoppa et al*., 1999]. Furthermore, the pattern of strike-slip faults on Enceladus suggests different stress mechanisms, or a combination of mechanisms, produced the observed fault distributions.

While only NSR was modeled here, there are a variety of other stress mechanisms relevant to icy satellites that can be explored to explain tectonic activity on Enceladus [e.g., *Kattenhorn and Hurford*, 2009; *Collins et al*., 2010]. In particular, polar wander [*Rhoden et al*., 2011, 2012] can produce stresses up to 10 MPa [*Nimmo and Pappalardo*, 2006; *Melosh*, 1980], which is sufficient to fracture Enceladus's ice shell. Polar wander may improve our understanding of strike-slip faulting on both Europa and Enceladus. If diapir-induced polar wander on Enceladus [*Nimmo and Pappalardo*, 2006] was the same event that induced the geologic activity within the SPT, and strike-slip faults on Enceladus were associated with the polar reorientation event, then

the initiation of strike-slip faulting was also recent, consistent with observations of strike-slip faults crosscutting many surrounding features. The presence of pit chains associated with strike-slip faults also suggests that there must have been loose regolith available on the surface which is actively being deposited by the south polar plume. *Matsuyama and Nimmo* [2008] explored the stress fields produced by various amounts of polar wander. They found that regions of shearing would occur in the present-day cratered terrains, consistent with the observed strike-slip fault distribution on Enceladus. Additionally, en echelon and tailcrack angles documented in this work suggest that dilation along strike-slip faults on Enceladus is a common component of motion. Further work is necessary to verify whether orientations of observed strike-slip faults on Enceladus and their sense of slip are consistent with modeled orientations caused by polar wander.

The lack of continuity between NSR and the distribution of strike-slip faults on Enceladus may also suggest that a regional stress field (or perturbation to a global stress field) is contributing to strike-slip faulting. An inherited crustal fabric, or motion along nearby, or subsurface faults, may be sufficient to perturb a remote stress field, similar to the way that stress concentrates at the tip of a strike-slip fault to produce tailcracks. Strike-slip faults on Earth have been shown to locally perturb a stress field causing slip along neighboring faults [*Stein et al*., 1992]. The 1992 Landers earthquake in California likely changed the stress field around the San Andreas Fault system [*Stein et al*., 1992], affecting motion around surrounding faults.

6. Conclusions

Strike-slip faults observed on Enceladus lack the lateral offsets typical of strike-slip faults on other icy bodies, such as Ganymede and Europa. However, en echelon cracks and/or tailcracks are diagnostic of strike-slip faults, and these secondary features were used to produce the first near-global map of strike-slip faults on Enceladus. Strike-slip faults are found primarily within the cratered terrains on the Saturn-facing and anti-Saturn hemispheres. They fall into three classes: tectonic terrain boundaries, reactivated linear features, and primary strike-slip faults. Formation of strike-slip faults on Enceladus is not consistent with formation within an NSR stress field. Polar wander and/or localized perturbations of the remote stress field (generated by proximal tectonic structures) are two possible alternative mechanisms, which require further investigation. The strike-slip faults bounding the leading hemisphere tectonized terrains suggest northward movement of the ice shell, perpendicular to the orientation of the present-day tiger stripes.

Acknowledgments

This work was funded by NASA Earth and Space Science Fellowship grant NNX11AP30H. E.S.M. would like to acknowledge Simon Kattenhorn, D. Alex Patthoff, and Jennifer Whitten for helpful discussion and two anonymous reviewers for their comments which served to significantly improve this manuscript. The data used are listed in the references, tables, supporting information, and The CEPS Data Repository at http://airandspace.si.edu/CEPSData.

References

Anderson, E. M. (1951), *The Dynamics of Faulting*, Oliver & Boyd, Edinburgh.

Barr, A. C., and L. J. Preuss (2010), On the origin of south polar folds on Enceladus, *Icarus*, 499–503, doi:10.1016/j.icarus.2010.03.038.

Bland, M. T., W. B. McKinnon, and P. M. Schenk (2015), Constraining the heat flux between Enceladus' Tiger Stripes: Numerical modeling of funiscular plains formation, *Icarus*, 232–245, doi:10.1016/j.icarus.2015.07.016.

Cloos, E. (1955), Experimental analysis of fracture patterns, *Bull. Geol. Soc. Am.*, *66*, 241–258, doi:10.1130/0016-7606(1955)66[241:EAOFP]2.0.CO;2.

Collins, G. C., W. B. McKinnon, J. M. Moore, F. Nimmo, R. T. Pappalardo, L. M. Prockter, and P. M. Schenk (2010), Tectonics of the outer planet satellites, in *Solar System Tectonics*, edited by T. Watters and R. Schultz, Cambridge Univ. Press, Cambridge, U. K.

Croft, S. K., J. S. Kargel, R. L. Kirk, J. M. Moore, P. M. Schenk, and R. G. Strom (1995), The geology of Triton, in *Neptune and Triton*, edited by D. P. Cruikshank, pp. 879–947, Univ. of Ariz. Press, Tucson, Ariz.

Crow-Willard, E. N., and R. T. Pappalardo (2015), Structural mapping of Enceladus and implications for formation of tectonized regions, *J. Geophys. Res. Planets*, *120*, 928–950, doi:10.1002/2015JE004818.

Cruikshank, K. M., and A. Aydin (1995), Unweaving the joints in Entrada Sandstone, Arches National Park, Utah, *J. Struct. Geol.*, *17*, 409–421, doi:10.1016/0191-8141(94)00061-4.

Cruikshank, K. M., G. Zhao, and A. M. Johnson (1991), Analysis of minor fractures associated with joints and faulted joints, *J. Struct. Geol.*, *13*, 865–886, doi:10.1016/0191-8141(91)90083-U.

Erdogan, F., and C. G. Sih (1963), On the crack extension in plates under plane loading and transverse shear, *J. Basic Eng.*, *85*, 519–527, doi:10.1115/1.3656897.

Groenleer, J. M., and S. A. Kattenhorn (2008), Cycloid crack sequences on Europa: Relationship to stress history and constraints on growth mechanics based on cusp angles, *Icarus*, *193*, 158–181, doi:10.1016/j.icarus.2007.08.032.

Hoppa, G., B. R. Tufts, R. Greenberg, and P. Geissler (1999), Strike-slip faults on Europa: Global shear patterns driven by tidal stress, *Icarus*, *141*, 287–298, doi:10.1006/icar.1999.6185.

Hurford, T. A., P. Helfenstein, G. V. Hoppa, R. Greenberg, and B. G. Bills (2007), Eruptions arising from tidally controlled periodic openings of rifts on Enceladus, *Nature*, *447*, 293–294, doi:10.1038/nature05821.

Hurford, T. A., P. Helfenstein, and J. N. Spitale (2012), Tidal control of jet eruptions on Enceladus as observed by Cassini ISS between 2005 and 2007, *Icarus*, *220*, 896–903, doi:10.1016/j.icarus2010.06.022.

Kargel, J. S., and S. Pozio (1996), The volcanic and tectonic history of Enceladus, *Icarus*, *119*, 385–404, doi:10.1006/icar.1996.0026.

Kattenhorn, S. A. (2002), Nonsynchronous rotation evidence and fracture history in the Bright Plains region, Europa, *Icarus*, *157*, 490–506, doi:10.1006/icar.2002.6825.

Kattenhorn, S. A. (2004), Strike-slip fault evolution on Europa: Evidence from tailcrack geometries, *Icarus*, *172*, 582–602, doi:10.1016/j.icarus.2004.07.005.

Kattenhorn, S. A., and T. A. Hurford (2009), Tectonics of Europa, in *Europa*, edited by R. T. Pappalardo, W. B. McKinnon, and K. Khurana, pp. 199–236, Univ. of Ariz. Press, Tucson, Ariz.

Kattenhorn, S. A., and S. T. Marshall (2006), Fault-induced perturbed stress fields and associated tensile and compressive deformation at fault tips in the ice shell of Europa: Implications for fault mechanics, *J. Struct. Geol.*, *28*, 2204–2221, doi:10.1016/j.jsg.2005.11.010.

Kay, J. P. (2010), The case for recent tectonic activity on Jupiter's moon Europa, Univ. of Idaho, Moscow, ID, Unpublished master's thesis.

Lawn, B. R., and T. R. Wilshaw (1975), *Fracture of Brittle Solids*, Cambridge Univ. Press, New York.

Marshall, S. T., and S. A. Kattenhorn (2005), A revised model for cycloid growth mechanics on Europa: Evidence from surface morphologies and geometries, *Icarus*, *177*, 397–412, doi:10.1016/j.icarus.2005.02.022.

Martin, E. S., and S. A. Kattenhorn (2014), A history of pit chain formation within Enceladus's cratered terrains suggests a nonsynchronous rotation stress field, *45th Lunar and Planetary Science Conferences*, Abstract 1083.

Matsuyama, I., and F. Nimmo (2008), Tectonic patterns on reoriented and despun planetary bodies, *Icarus*, *195*, 459–473, doi:10.1016/j.icarus.2007.12.003.

Melosh, H. J. (1980), Tectonic patterns on a reoriented planet: Mars, *Icarus*, *44*(3), 745–751, doi:10.1016/0019-1035(80)90121-4.

Michaud, R. L., R. T. Pappalardo, and G. C. Collins (2008), Pit chains on Enceladus: A discussion of their origin, *39th LPSC*, Abs. 1678.

Nicholson, R., and D. D. Pollard (1985), Dilation and linkage of echelon cracks, *J. Struct. Geol.*, *7*(5), 583–590, doi:10.1016/0191-814(85)90030-6.

Nimmo, F., and R. T. Pappalardo (2006), Diapir-induced reorientation of Saturn's moon Enceladus, *Nature*, *441*, 614–616, doi:10.1038/nature04821.

Nimmo, F., J. R. Spencer, R. T. Pappalardo, and M. E. Mullen (2007), Shear heating as the origin of the plumes and heat flux on Enceladus, *Nature*, *447*, 289–291, doi:10.1038/nature05783.

Nimmo, F., C. Porco, and C. Mitchell (2014), Tidally modulated eruptions on Enceladus: *CASSINI* ISS observations and models, *Astron. J.*, *148*, 46, doi:10.1088/0004-6256/148/3/46.

Olson, J. E., and D. D. Pollard (1991), The initiation and growth of en echelon veins, *J. Struct. Geol.*, *13*(5), 595–608, doi:10.1016/0191-814(91)90046-L.

Pappalardo, R. T., et al. (1998), Grooved terrain on Ganymede: First results from 8 Galileo high-resolution imaging, *Icarus*, *135*, 276–302, doi:10.1006/icar.1998.5966.

Patthoff, D. A., and S. K. Kattenhorn (2011), A fracture history on Enceladus provides evidence for a global ocean, *Geophys. Res. Lett.*, *38*, L18201, doi:10.1029/2011GL048387.

Patthoff, D. A., R. T. Pappalardo, J. Li, B. Ayton, J. P. Kay, and S. A. Kattenhorn (2015), Modeling tidal stresses on satellites using an enhanced SatStressGUI, *Eos*, *Trans*. *AGU* 96, Fall Meet. Suppl., Abstract P31C-2079.

Pollard, D. D., and A. Aydin (1988), Progress in understanding jointing over the past century, *Geol. Soc. Am. Bull.*, *100*, 1181–1204, doi:10.1130/0016-7606(1988)100<1181:PIUJOT>2.3.CO;2.

Pollard, D. D., and P. Segall (1987), Theoretical displacements and stresses near fractures in rock: With applications to faults, joints, veins, dikes, and solution surfaces, in *Fracture Mechanics of Rock*, edited by B. K. Atkinson, pp. 277–349, Academic Press, London.

Pollard, D. D., P. Segall, and P. Delaney (1982), Formation and interpretation of dilatant echelon cracks, *Bull. Geol. Soc. Am.*, *93*, 1291–1303, doi:10.1130/0016-7606(1982)93<1291:FAIODE>2.0.CO;2.

Porco, C. C., et al. (2006), Cassini observes the active south pole of Enceladus, *Science*, *311*, 1393–1401, doi:10.1126/science.1123013.

Porco, C., D. DiNino, and F. Nimmo (2014), How the geysers, tidal stresses, and thermal emission across the south polar terrain of Enceladus are related, *Astron. J.*, *148*, 45, doi:10.1088/0004-6256/148/3/45.

Ramsay, J. G. (1980), The crack-seal mechanism of rock deformation, *Nature*, *284*, 135–139, doi:10.1038/284135aO.

Rhoden, A. R., T. A. Hurford, and M. Manga (2011), Strike-slip fault patterns on Europa: Obliquity or polar wander?, *Icarus*, *211*, 636–647, doi:10.1016/j.icarus.2010.11.002.

Rhoden, A. R., G. Wurman, M. Manga, E. M. Huff, and T. A. Hurford (2012), Shell tectonics: A mechanical model for strike-slip displacement on Europa, *Icarus*, *218*(1), 297–307, doi:10.1016/j.icarus.2011.12.015.

Rhoden, R. R., and T. A. Hurford (2013), Lineament azimuths on Europa: Implications for obliquity and non-synchronous rotation, *Icarus*, *226*, 841–859, doi:10.1016/j.icarus.2013.06.029.

Riedel, W. (1929), Zur mechanic geologischer Brucherscheinungen (Ein Beitrag zum Problem der Fiederspatten), *Zentbl. Miner. Geol. Paläeont. Abt. B*, 354–368.

Roatsch, T., E. Kersten, A. Hoffmeister, M. Wählisch, K.-D. Matz, and C. C. Porco (2013), Recent improvements of the Saturnian satellites atlases: Mimas, Enceladus, and Dione, *Planet. Space Sci.*, *77*, 118–125, doi:10.1016/j.pss.2012.02.016.

Sarid, A. R., R. Greenberg, G. V. Hoppa, T. A. Hurford, B. R. Tufts, and P. Geissler (2002), Polar wander and surface convergence of Europa's ice shell: Evidence from a survey of strike-slip displacement, *Icarus*, *158*, 24–41, doi:10.1006/icar.2002.6873.

Schulson, E. M., and P. Duvall, (2009), *Creep and Fracture of Ice*, 416 pp., Cambridge Univ. Press, Cambridge, U. K., doi:10.1017/CBO9780511581397.

Smith, B. A., et al. (1989), Voyager 2 at Neptune: Imaging science results, *Science*, *246*, 1422, doi:10.1126/science.246.4936.1422.

Smith-Konter, B., and R. T. Pappalardo (2008), Tidally driven stress accumulation and shear failure of Enceladus's tiger stripes, *Icarus*, *198*, 435–451, doi:10.1016/j.icarus.2008.07.005.

Sommer, E. (1969), Formation of fracture lances in glass, *Eng. Fract. Mech.*, *1*, 539–546, doi:10.1016/0013-7944(69)90010-1.

Spencer, J. R., A. C. Barr, L. W. Esposito, P. Helfenstein, A. P. Ingersoll, R. Jaumann, C. P. McKay, F. Nimmo, and J. H. Waite (2009), Enceladus: An active cryovolcanic satellite, in *Saturn after Cassini-Huygens*, pp. 683–722, Springer, New York.

Spitale, J. N., and C. C. Porco (2007), Association of the jets of Enceladus with the warmest regions on its south-polar fractures, *Nature*, *449*, 695–697, doi:10.1038/nature06217.

Stein, R. S., G. C. P. King, and J. Lin (1992), Change in failure stress on the southern San Andreas Fault system caused by the 1992 magnitude = 7.4 Landers earthquake, *Science*, *258*, 1328–1332, doi:10.1126/science.258.5086.1328.

Wahr, J., Z. A. Selvens, M. E. Mullen, A. C. Barr, G. C. Collins, M. M. Selvans, and R. T. Pappalardo (2009), Modeling stresses on satellites due to nonsynchronous rotation and orbital eccentricity using gravitational potential theory, *Icarus*, *200*(1), 188–206, doi:10.1016/j.icarus.2008.11.002.

Willemse, E. J. M., D. C. P. Peacock, and A. Aydin (1997), Nucleation and growth of strike-slip faults in limestone from Somerset, U. K., *J. Struct. Geol.*, *19*, 1461–1477, doi:10.1016/S0191-814(97)00056-4.

Wyrick, D., D. A. Ferrill, A. P. Morris, S. L. Colton, and D. W. Sims (2004), Distribution, morphology, and origins of Martian pit crater chains, *J. Geophys. Res.*, *109*, E06005, doi:10.1029/2004JE002240.

Yin, A., and R. T. Pappalardo (2015), Gravitational spreading, bookshelf faulting, and tectonic evolution of the south polar terrain of Saturn's moon Enceladus, *Icarus*, *260*, 409–439, doi:10.1016/j.icarus.2015.07.017.